Research Article

For reprint orders, please contact: reprints@future-science.com

Future Medicinal Chemistry

Benzodifurans for biomedical applications: BZ4, a selective anti-proliferative and anti-amyloid lead compound

Caterina Vicidomini[1], Federica Cioffi[2], Kerensa Broersen[2], Valentina Roviello[3], Claudia Riccardi[4], Daniela Montesarchio[4], Domenica Capasso[5], Sonia Di Gaetano[1], Domenica Musumeci*,[1,4] & Giovanni N Roviello**,[1]

[1]CNR, Institute of Biostructure & Bioimaging, Via Mezzocannone site & Headquarters, 80134 Naples, Italy
[2]Nanobiophysics, Faculty of Science & Technology (TNW), Technical Medical Centre, University of Twente, The Netherlands
[3] Advanced Metrologic Service Center (CeSMA), University of Naples Federico II, Corso N. Protopisani, 80146 Naples, Italy
[4]Department of Chemical Sciences, University of Naples Federico II, Via Cintia 21, 80126 Naples, Italy
[5]Department of Pharmacy, University of Naples Federico II, Via Mezzocannone 16, 80134 Naples, Italy
*Author for correspondence: Tel.: +39 (0)81 674 143; Fax: +39 (0)81 674 141; domenica.musumeci@unina.it
**Author for correspondence: Tel.: +39 (0)81 253 4585; Fax: +39 (0)81 253 4574; giroviel@unina.it; giovanni.roviello@cnr.it

Aim: Our goal is to evaluate benzodifuran-based scaffolds for biomedical applications. **Methodology:** We here explored the anticancer and anti-amyloid activities of a novel compound (BZ4) in comparison with other known benzodifuran analogs, previously studied in our group, and we have explored its ability to interact with different DNA model systems. **Results:** BZ4 shows antiproliferative activity on different cancer cells; does not affect noncancerous control cells and alters the aggregation properties of β-amyloid, as ascertained by circular dichroism, fluorescence spectroscopy and scanning electron microscopy analysis. An overall, qualitative picture on the mechanistic aspects related to the biological activities is discussed in light of the dynamic light scattering, UV, circular dichroism and fluorescence data, as well as of the metal ion-binding properties of BZ4.

Graphical abstract:

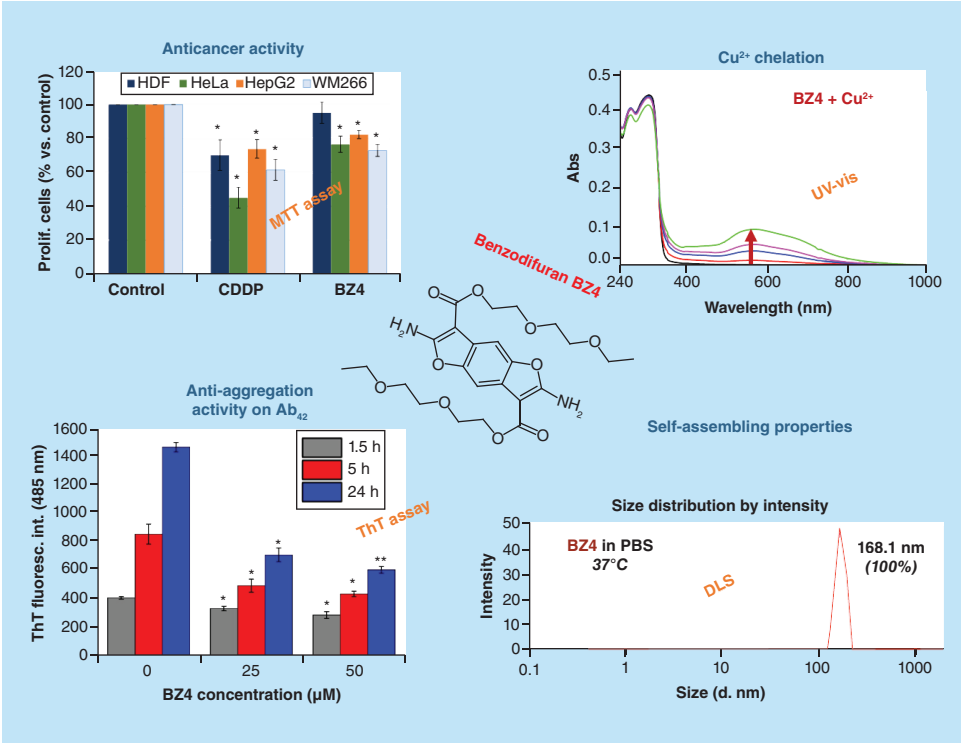

newlands press

First draft submitted: 21 September 2018; Accepted for publication: 30 November 2018; Published online: 25 February 2019

Keywords: anti-amyloid • anticancer • synthesis

Benzofuran derivatives are heterocyclic compounds found in natural sources, as well as synthetic materials, that have been extensively studied as therapeutic agents for several cancer forms, showing a marked therapeutic activity associated to their binding to receptors like estrogen receptor-α (ERα) [1] and to their potent aromatase inhibitory activity [2,3]. Due to the increasing need to develop new effective anticancer drugs and taking into account the great potential provided in this field by benzofuran compounds, we aimed at exploring the anticancer potential of their tricyclic analogs, benzodifurans. These compounds are mostly investigated in the field of new materials, especially as organic dyes in the development of solar cells [4], and only few studies have been addressed thus far at the investigation of their biological activity [5–7]. Recently, the synthesis and structural characterization of various substituted benzodifuran derivatives, as well as their biological activities have been reported in the literature. These compounds showed interesting antiproliferative effects on different cancer cell lines, also with cell-selective activity [8]. They formed nanoaggregates stable at physiological temperature, probably responsible for their bioactivity, as evidenced for other self-assembling biologically active molecules [9]. Among the three novel benzodifurans previously described, only **BZ1** (Figure 1) was able to bind Cu^{2+} ions, suggesting that copper ion depriving ability is not a mechanism of action common to all these compounds and that probably each benzodifuran derivative exerts cytotoxic effects by virtue of specific mechanisms or different combinations of them [8]. Overall, these benzodifuran derivatives proved to be valuable lead compounds in anticancer therapies, but their poor solubility (in some cases limited also in dimethyl sulfoxide) impaired further investigations.

Thus, with the aim of improving the solubility properties of **BZ1**, that is the most promising compound among the previously investigated benzodifuran derivatives, we here designed a new analog with longer oligoethylene glycol chains, named **BZ4** (Figure 1), which could confer better solubility properties and in general a good hydrophilic–lipophilic balance for the studied scaffold, as previously demonstrated in the case of other small molecules [10–12].

We here report the synthesis and characterization, by spectroscopic and spectrometric techniques, of **BZ4**, as well as the evaluation of its biological properties. In particular, in analogy with previous works and in continuation with studies on the search for effective antineoplastic small molecules [13,14], we explored the antiproliferative activity of **BZ4** on different human cancer and normal control cells, comparing the observed effects with those previously associated to **BZ1**, **BZ2** and **BZ3** derivatives (Figure 1) [8]. Furthermore, aiming at shedding light on the potential biological targets and mechanisms at the origin of the biological activity of **BZ4**, we evaluated the ability of **BZ4** to bind various DNA model systems (in single strand, duplex and G-quadruplex forms) and/or biologically relevant Cu^{2+} ions, as well as its aggregation properties.

Moreover, we evaluated also the interaction of **BZ4** with the β-amyloid (Aβ) peptide, a peptide related to a number of pathologies, using different techniques. Aggregation and deposition of Aβ peptide leads to pathogenic plaques observed in the brain of Alzheimer's disease (AD) patients, the most common form of neurodegenerative diseases [15]. $Aβ_{40}$ and $Aβ_{42}$ are the two prevailing isoforms of Aβ peptide in the human brain, of which the longer $Aβ_{42}$ isoform more readily self-assembles into aggregates [15,16]. Aggregation of $Aβ_{42}$ peptides is an early event in the disease progression of AD. Thus, any strategy interfering with the Aβ self-assembly is potentially of high therapeutic interest in order to retard or prevent AD onset [16]. Several compounds of different nature were identified in the past as effective inhibitors of amyloid formation [17,18], and among these, a pivotal role is played by aromatic or heteroaromatic compounds such as curcumin or quinone derivatives [19,20]. Furthermore, amyloid-induced toxicity on neuronal cells was prevented by microRNAs, sulfonates and liposomes [21–23], while gold nanoparticles were successfully employed to visualize $Aβ_{42}$ aggregation, thus providing new tools in diagnostic and prognostic strategies for neurodegenerative disease treatment [24]. Interestingly, compounds containing benzofuran moieties have been described to bind amyloid plaques, as well as neurofibrillary tangles [25] and can play an important role in decreasing Aβ-induced toxicity by interfering with Aβ binding to plasma membrane [26], as well as inhibiting Aβ aggregation [27,28]. The latter effect on Aβ produced by benzofuran derivatives is closely related with their ability to directly bind the Aβ and is associated with their intrinsic self-aggregation tendency [29]. Additionally, a specific recognition site for benzofurans on Aβ, different from those of nonbenzofuran Aβ disaggregators, is involved during their interference process on amyloid fibril formation [29].

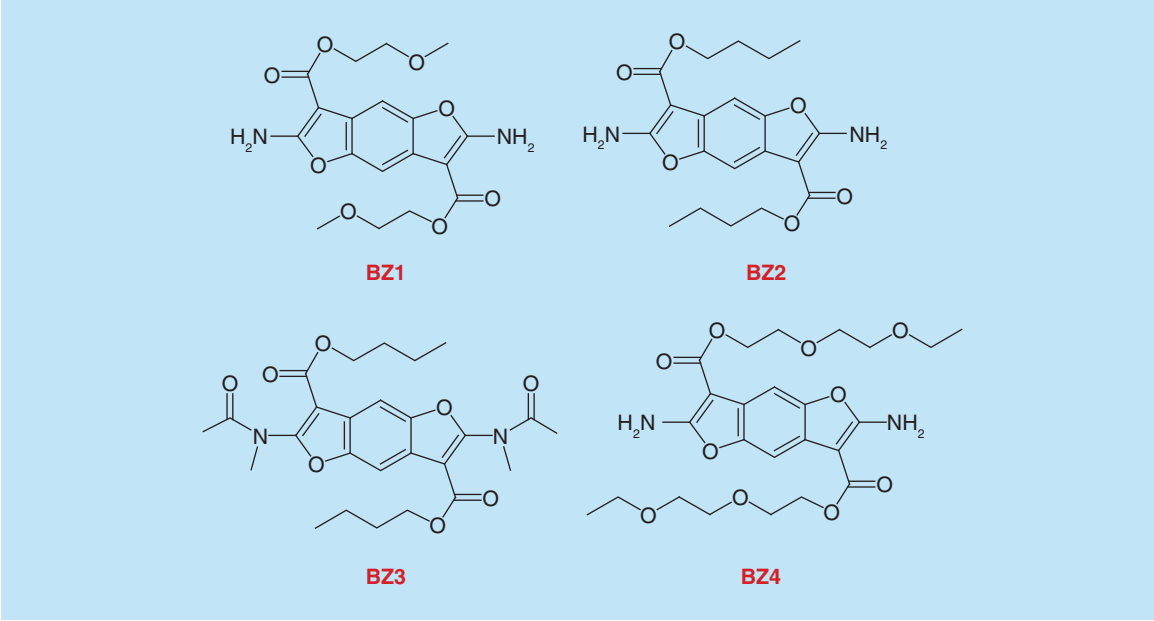

Figure 1. Chemical structure of BZ1, BZ2, BZ3 and BZ4 derivatives.

Benzofuran-based derivatives were previously shown to interact with *in vitro*-generated Aβ40 aggregates with subnanomolar binding affinity [30]. However, these compounds also showed slow wash out and long retention in the brains of control mice suggesting nonspecific interaction with brain constituents other than Aβ aggregates. Redesign of benzofuran-based derivatives aimed at retaining their high binding affinity but improving their selectivity is thus beneficial.

In this context, the introduction of a third fused furan cycle is a chemical modification of the starting benzofuran scaffold never tested before, whose effect on amyloid aggregation and toxicity on primary mouse cortical neurons is also the object of the present study.

Thus, aiming at the development of specific $A\beta_{42}$-targeting neurodrugs, the anti-amyloid activity of benzodifurans, unprecedentedly explored, was here studied. The $A\beta_{42}$ anti-aggregation potential of **BZ4** as well as of the previously described benzodifurans [8] were evaluated by means of fluorescence assays (thioflavin T, ThT). The benzodifuran-$A\beta_{42}$ interaction and consequent amyloid anti-aggregation effect were confirmed by circular dichroism (CD) and scanning electron microscopy (SEM) microscopy studies.

Experimental section

Abbreviations

Alzheimer's disease (AD); circular dichroism (CD); dimethyl sulfoxide (DMSO); Dulbecco's Modified Eagle's Medium (DMEM); dynamic light scattering (DLS); fetal bovine serum (FBS); human cervix adenocarcinoma cells (HeLa); liver hepatocellular carcinoma (Hep-G2); 4-(2-hydroxyethyl)-1-piperazineethanesulfonic acid (HEPES); human dermal fibroblast (HDF); liquid chromatography-electrospray ionization-mass spectrometry (LC–ESI/MS); 3-(4,5-dimethylthiazol-2-yl)-2,5-diphenyltetrazolium bromide (MTT); nuclear magnetic resonance (NMR); oligodeoxyribonucleotide (ODN); phosphate-buffered saline (PBS); scanning electron microscopy (SEM); thioflavin T (ThT); melting temperature (T_m); total ion current (TIC); time of flight (TOF) and malignant melanoma (WM266).

Materials & methods

All chemicals and solvents were purchased from Sigma-Aldrich (Amsterdam, The Netherlands).

Human cervix adenocarcinoma cells (HeLa), liver hepatocellular carcinoma (Hep-G2) and malignant melanoma (WM266) cells were obtained from ATCC (Manassas, VA, USA). Human dermal fibroblasts (HDFs) were a kind gift from Dr Annalisa Tito (Arterra Biosciences, NA, Italy).

TLC analyses of the benzodifuran derivatives were performed on SiO_2 aluminium-supported plates from Macherey–Nagel (60, F254 – from Delchimica S.G. Srl, NA Italy) using the mixture CH_2Cl_2/CH_3OH 95:5 (v/v) as eluent.

All the oligonucleotide sequences listed below were prepared by using standard phosphoramidite solid phase synthesis (ABI Expedite 8909 synthesizer) on the scale of 1 μmol:

– d($^{5'}$CCTCTGGTCTCC$^{3'}$) (**A**);

– d($^{5'}$GGAGACCAGAGG$^{3'}$) (**B**);

– d[$^{5'}$TCACACACACACACACACACACTT$^{3'}$] (**C**);

– d[$^{5'}$(TTAGGG)$_4$TT$^{3'}$] (**tel$_{26}$**).

Deprotection and detachment of the oligodeoxyribonucleotides (ODNs) from the resin were obtained by treatment with ammonia (aq.) at 55°C for 12 h, after which the oligomers were purified by C18 cartridges (GlenPack of GlenRes, purchased from Primm Srl, MI Italy), desalted by dialysis versus H_2O and lyophilized.

^{1}H and ^{13}C NMR spectra were recorded on a Bruker WM-400 spectrometer using DMSO-d_6 as solvent. All chemical shifts (δ) are expressed in parts per million (ppm) with respect to the residual solvent signal both for ^{1}H NMR [DMSO-d_6 = 2.50 ppm] and ^{13}C NMR (DMSO-d_6 = 39.5 ppm). All the coupling constants (*J*) are quoted in Hertz (Hz).

Abbreviations used for the multiplicities are: s = singlet; d = doublet; t = triplet; q = quartet; m = multiplet; b = broad.

LC–MS ESI–TOF analysis on the final purified benzodifuran **BZ4** was carried out on an Agilent 6230B TOF LC–MS system, composed of a HPLC analytical system (1260 Infinity) with binary pump and a TOF–MS as detector with an ESI source. Reverse phase HPLC was performed on a C18 column (Agilent ZORBAX from Agilent Technologies, MI Italy, 1.8 μm, 50 × 4.6 mm). The benzodifuran samples for analysis were prepared by withdrawing 1 μl of a 2 mM solution of the compound in DMSO and diluting it to 500 μl H_2O; 20 μl injections of these solutions were analyzed with a flow rate of 0.4 ml/min. Column elution was conducted by using H_2O (A) and CH_3CN (B) as eluents. Gradient: from 5% B in A to 95% B over 5 min and 95% B in A for 3 min. The MS analysis was operated in the positive ion mode (100–1000 m/z range).

The UV-vis experiments were carried out on a UV-vis spectrophotometer JASCO (Easton, MD USA) V-550 coupled to a Peltier Thermostat JASCO ETC-505T by using a quartz cuvette with a path length of 1.0 cm (internal volume = 1.0 ml). The spectra, subtracted of the appropriate baseline, were recorded with the following parameters: medium response, 100 nm/min scanning speed, 2.0 nm bandwidth. A scan rate of 1°C/min and a fixed absorbance value was used for the temperature-scanning UV measurements. The concentrations of the oligonucleotides were obtained by measuring the absorbance values at 260 nm and 85°C of solutions obtained by dissolving the oligomers in a known bidistilled H_2O volume. The melting temperature value of the duplex was calculated by the first derivative method.

CD experiments were carried out in analogy with previous studies [31,32]. CD spectra were obtained on a Jasco J-715 spectropolarimeter coupled to a PTC-348WI temperature control system.

SEM: few drops of the benzodifuran samples eluted in tetrahydrofuran were dried on Al stubs and coated with Au and Pd for the microscopic observations, using a Scanning Electron Microscope (Nova NanoSem 450, FEI-Thermo Fisher – Thermo Fisher Scientific, MA USA).

The dynamic light scattering (DLS) measurements were performed on a Zetasizer Nano ZSP (Malvern Instruments, Worcerstershire, UK) equipped with a temperature controller. Solutions of the benzodifurans at 10 μM concentration were prepared by diluting 2 mM stock solutions of the compounds dissolved in DMSO to 1 ml PBS buffer (140 mM NaCl, 10 mM phosphate buffer and 3 mM KCl) previously filtered on a 0.2 μm filter The data were collected at a scattering angle of 173° at a given temperature until stabilization of the signal and carried out in triplicate.

Emission fluorescence spectra (5 nm slit widths), from 370 to 570 nm, of **BZ4** at 7 μM concentration were recorded in PBS at 20°C, by using a quartz cuvette with a path length of 1 cm and a 0.5 ml volume capacity. The excitation wavelength was 314 nm.

Synthesis of 2,6-diamino-benzo[1,2-b;4,5-b']difuran-3,7-dicarboxylic acid bis-[2-(2-ethoxy-ethoxy)-ethyl] ester (BZ4)

For the synthesis of **BZ4**, 2-(2-ethoxyethoxy)ethyl 2-cyanoacetate (**2**) was first prepared as depicted in Supplementary Scheme 1. Then, 4.5 ml of the crude ester **2** were added to a solution of 1,4-benzoquinone (0.5 g, 4.6 mmol)

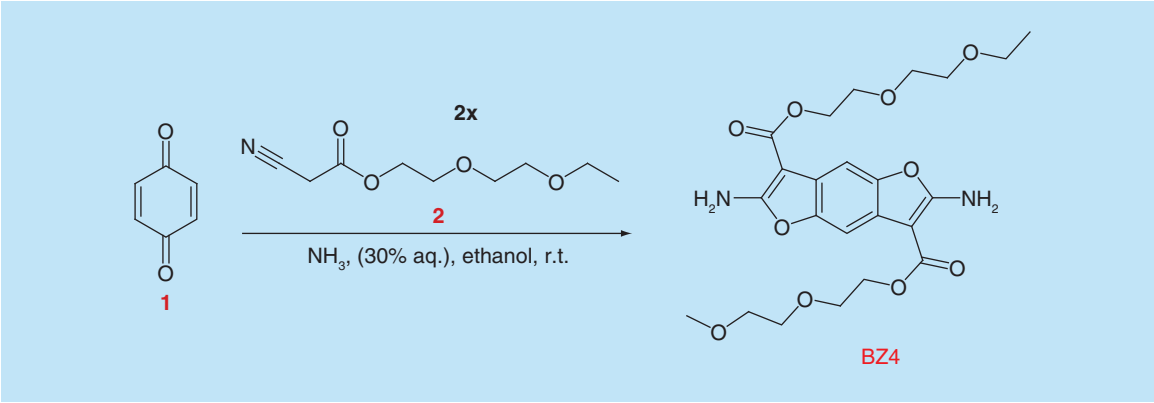

Figure 2. Synthetic scheme for the preparation of the benzodifuran derivative BZ4, starting from 1,4-benzoquinone (1) and cyanoacetate ester derivative 2.
aq.: Aqueous; r.t.: Room temperature.

in absolute ethanol (4.0 ml) and the resulting mixture left under stirring at room temperature. The addition of 30% aqueous ammonia solution (3.0 ml) caused a fast exothermic reaction, with temperature rising up to 40°C. After 2 h, ethanol and ammonia were removed under reduced pressure and 15 ml of water were added. A dark grey solid precipitate was recovered by filtration under vacuum and purified by crystallization using ethanol/acetone: 0.55 g (23% yield) of a product, identified as **BZ4** by NMR and LC–MS analyses, were obtained. The synthetic procedure is outlined in Figure 2.

^{1}H NMR (400 MHz, DMSO-d_6): δ 7.65 (s, 4H), 7.36 (s, 2H), 4.32 (t, J 4.8 Hz, 4H), 3.76 (t, J 4.8 Hz, 4H), 3.60 (t, J 4.6 Hz, 4H), 3.51 (t, J 4.8 Hz, 4H), 3.43 (m, 4H), 1.06 (t, J 7.0 7.0 Hz, 6H).

^{13}C NMR (100 MHz, DMSO-d_6): δ 165.1, 164.2, 145.7, 121.1, 99.6, 81.8, 69.8, 69.2, 68.7, 65.6, 61.9, 15.1.

LC–ESI/MS: m/z 509.2 $(M+H)^+$, 1017.4 $(2M+H)^+$, 1039.3 $(2M+Na)^+$, t_R = 5.02 min.

TLC (CH_2Cl_2/CH_3OH, 95:5 v/v) R_f = 0.70.

MTT assays on HeLa, Hep-G2, HDF, WM266 cells

HeLa, Hep-G2 and HDF cells were maintained in DMEM and WM266 in RPMI with 10% FBS, 2 mM L-glutamine, 100 µg/ml penicillin and 100 µg/ml streptomycin, in a humidified incubator at 5% CO_2 at 37°C [33].

BZ4 (10 mg) was further purified on a prepacked C18 minicolumn and 2 mg of the collected compound were dissolved in DMSO, so to have a 2 mM stock solution. Cisplatin was dissolved in 0.9% NaCl aq. solution.

A total of 2500 HDF cells and 3000 for all the other cancer cell lines were plated in 96-well tissue culture microplates and incubated at 37°C for 24 h. The benzodifuran or cisplatin solution was added to the cells at the proper concentration. As control, an equal amount of DMSO or 0.9% NaCl, respectively, was used. MTT assay was performed after 24 h of treatment [34]. In detail, for each well, 100 µl of a MTT solution at a 0.5 mg/ml final concentration, diluted in medium without red phenol, was added and incubated for 4 h. Then, the solution was discarded and formazan crystals were dissolved in isopropanol containing TRITON-X100 10% and HCl (0.04–0.1 N). Finally, the absorbance was determined at 570 nm by an automated spectrophotometric plate reader. The experiment was performed at least in triplicate.

Primary cortical neuron culture preparation

These cultures were prepared from E14–E16 mouse embryonic brains. Cells were seeded in a 96-well plate at 60,000 cells/well on polyethylenimine (PEI) precoated plates. To prepare the culture medium, neurobasal medium (Gibco, Landsmeer, The Netherlands) was supplemented with the 2% (v/v) of B27-supplement, glutamine at a concentration of 0.5 mM) and 0.2% Penicillin-Streptomycin [P/S] – ThermoFisher Scientific, Landsmeer, The Netherlands). Cells were first cultured in this medium for 48 h after which cytosine arabinoside (Sigma) was added at a concentration of 10 µM for 24 h in order to inhibit the growth of nonneuronal cells. Afterward, the medium was substituted with fresh neurobasal medium and after a week the neuronal cells (<1% contaminating glial cells) were treated for the MTT assay performed as described before.

Circular dichroism experiments

The CD spectra were registered in a quartz cell with a path length of 1 cm, at 20°C or 37°C (for $A\beta_{42}$ binding experiments) with a response of 1 s, a scanning speed of 100 nm/min and a 2.0 nm bandwidth. All the spectra were averaged over three scans.

For the experiments with DNA, a 2 μM solution of the oligonucleotide – dissolved in PBS containing NaH_2PO_4 (10 mM) and KCl (100 mM), pH = 7.2 – and a benzodifuran 1.5 mM stock solution in DMSO were used. The CD titration curves were recorded after the addition of increasing aliquots of the ligand (0.5 equiv. at a time, 0.65 μl) up to 5 equiv. (10 μM concentration) to the various DNA solutions. Each sample addition was followed by a suitable equilibration time after which the spectra were recorded. In all cases, no DMSO contribution to the oligonucleotide CD spectra was detected. We obtained the melting curves recording the CD at 290 nm (in case of G4) or 276 nm (for duplex DNA) upon temperature increase with a scan rate of 1°C/min. T_m values were obtained by the first derivative method.

Experiments with $A\beta_{42}$ were carried out using a 5 μM concentration of $A\beta_{42}$ in PBS (overall volume = 2 ml, pH 7.2) and a twofold concentration of **BZ4**. All samples were incubated at 37°C for 0, 24 and 48 h.

Copper(II) binding experiments

The binding experiments were monitored by UV/Vis spectroscopy as follows: **BZ4** was used at 25 μM in PBS at 25°C and pH 7.2, in order to have a stable UV signal over the experiment period; then, the addition of two equivalents of a Cu^{2+} solution (withdrawn from a 10 mM stock solution of copper(II) chloride) was carried out. Thereafter UV/Vis spectra were registered for an overall period of 3 h subsequent the addition of the metal salt. Each experiment was performed in duplicate.

Aβ peptide solubilization

Solutions of recombinant $A\beta_{42}$ peptide (rPeptide, GA, USA) were prepared according to a previously published procedure [35]. In short, Aβ was sequentially dissolved in hexafluoroisopropanol (HFIP) and DMSO. The DMSO was removed from the Aβ solution by using a HiTrap™ desalting column (GE Healthcare, Zwijndrecht, The Netherlands) and elution with PBS at pH 7.4. We measured the $A\beta_{42}$ concentration by the Coomassie (Bradford, UK) Protein Assay Kit (ThermoFisher, Landsmeer, The Netherlands) and, afterward, the final concentration required for the subsequent experiments was achieved after dilution. Aβ peptide aggregation, in the presence or absence of **BZ4**, was evaluated at 37°C under quiescent conditions.

Thioflavin-T assay

Amyloid fibril formation was measured by a ThT fluorescence assay. We adjusted the $A\beta_{42}$ concentration to 25 μM diluting the peptide solution with PBS buffer (pH 7.4), while a final ThT concentration of 12 μM was realized in a 96-well plate (Greiner flat bottom transparent black, Sigma – cat. M9685). The emitted fluorescence intensity of ThT was measured upon excitation at a wavelength of 450 nm by detection in the range 480–600 nm. The fluorescence intensity from ThT at its maximum (485 nm) was reported in a graph in dependence of the different concentrations of **BZ4**. We performed measurements in triplicate, averaged the values recorded and subtracted background measurements that corresponded to buffer containing 12 μM ThT and the tested benzodifuran compound.

Molecular models

Energy-minimized 3D structure models (random low energy conformers) were obtained by DataWarrior (http://openmolecules.org/) and MOLVIEW (http://molview.org) softwares. Molecular volume of **BZ4** was estimated by Molinspiration (http://www.molinspiration.com).

SEM analysis

The samples for microscopic observations were derived from CD experiment solutions. The solvent was left to slowly evaporate, and then, pure **BZ4**, $A\beta_{42}$, and mixture of **BZ4** and $A\beta_{42}$, were coated on a conductive layer of Au–Pd. Then, the prepared samples were analyzed on a Nova NanoSem 450 FEI SEM instrument using a kilovolt ranging from 2.00 to 5.00 in high vacuum.

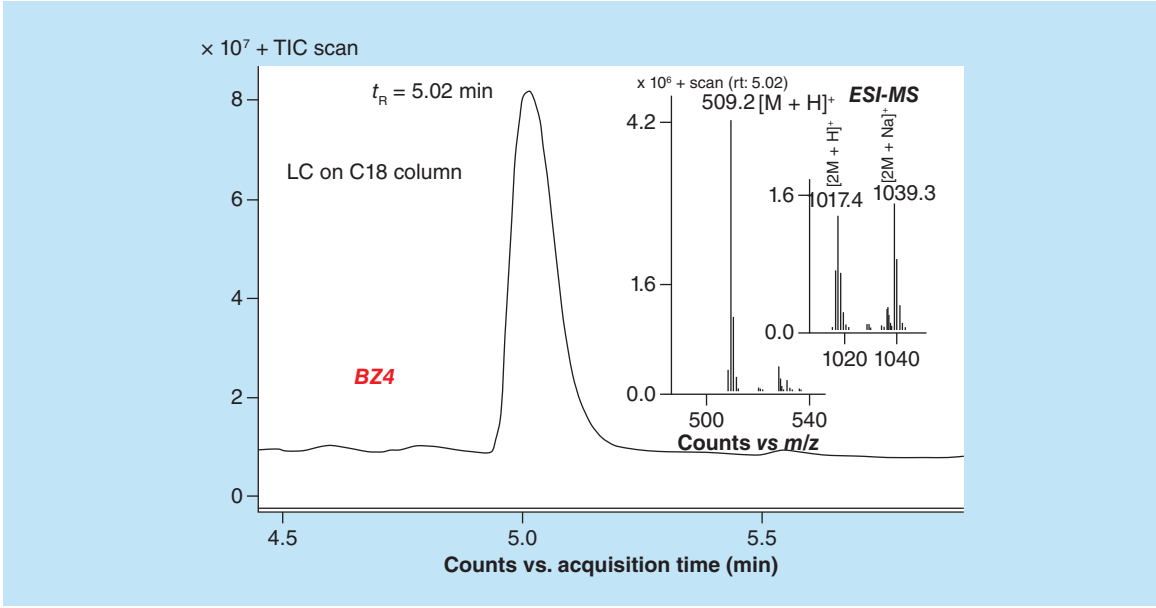

Figure 3. Total ion current chromatogram and ESI–TOF (positive ion mode) mass spectrum of BZ4.
ESI-MS: Electrospray ionization mass spectrometry; LC: Liquid chromatography; m/z: Mass/charge; M: Molecular mass; t_R: Retention time; TIC: Total ion current chromatogram; TOF: Time of flight; rt: Room temperature.

Results & discussion

Design, synthesis & characterization of the new benzodifuran derivative BZ4

In order to improve the solubility in aqueous solutions and the general hydrophilic–lipophilic balance of **BZ1** (Figure 1), in other words, the most promising among the benzodifuran derivatives we have previously investigated [8], we here designed **BZ4**. With respect to the original compound, this new derivative carries longer oligoethylene glycol chains, attached through stable ester bonds to the central benzodifuran scaffold.

In our design, intramolecular H-bonds formed between the ethylene glycol chains with NH_2 residues should be somehow prevented by their tendency to point in different directions (Supplementary Figure 1). Thus, potential intermolecular associations can be driven by both chains and benzodifuran moiety, the latter being able to in principle interact via π–π stacking with other aromatic molecules (e.g., nucleic acid bases or other **BZ4** units) leading to potentially relevant complexes or self-assemblies.

For the synthesis of the target compound containing two free amino groups and two ethylene glycol chains, respectively, in 2 (and 2′) and 3 (3′) positions of the benzodifuran core, a recent protocol based on the Craven reaction, in analogy to a previous work [8], was employed. Starting materials were the commercially available 1,4-benzoquinone (**1**; Figure 2) and the *ad hoc* synthesized 2-(2-ethoxyethoxy)ethyl 2-cyanoacetate ester (**2**; Supplementary Scheme 1) mixed in 1:2 ratio in the presence of ammonia (30% aq.) and ethanol. This one-pot reaction, depicted in Figure 2, allowed obtaining the target **BZ4**, which was then purified after a simple work-up, consisting of precipitation from water and crystallization from ethanol/acetone and isolated as a pure compound in a 23% yield.

Compound **BZ4** was analyzed and characterized by LC–ESI/MS (Figure 3 & Supplementary Figure 2A) and $^1H/^{13}C$ NMR (Supplementary Figures 2B & 3) techniques, which confirmed the identity and purity of the desired product. The higher polarity of **BZ4** compared with its analog **BZ1** was evidenced by its lower R_f on a TLC silica plate (eluent = CH_2Cl_2/CH_3OH, 95:5 v/v; **BZ4** R_f = 0.70; **BZ1** R_f = 0.77).

Then the spectroscopic properties of the benzodifuran derivative, dissolved in an aqueous saline buffer, were analyzed by UV and fluorescence spectroscopies. The UV spectrum of a 7 μM solution of **BZ4** in PBS buffer at room temperature showed two absorption bands at 314 and 269 nm (Figure 4A) which were approximately stable over 4 h monitoring (Supplementary Figure 4) after dilution of the compound from a concentrated stock solution in DMSO. The fluorescence spectrum of **BZ4** showed an emission band of low intensity at 426 nm upon excitation at 314 nm (Figure 4B).

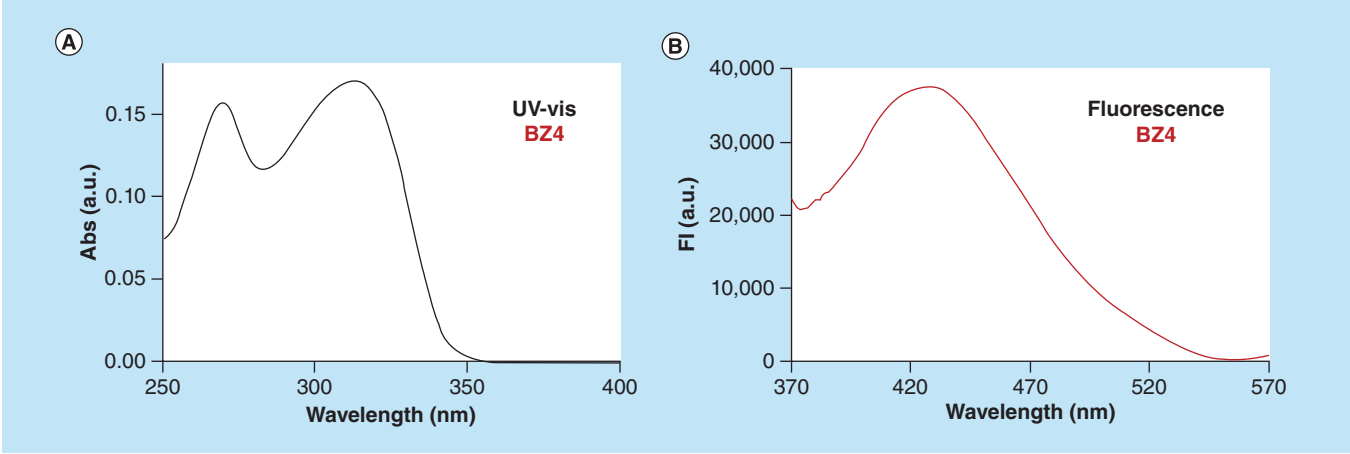

Figure 4. Spectroscopic analysis of BZ4. (A) UV and **(B)** fluorescence spectra of a 7 μM solution of **BZ4** in phosphate-buffered saline (containing ca. 0.1 % of DMSO) recorded at room temperature.

Aggregation properties of BZ4 in solution

In order to investigate the self-assembling behavior of **BZ4** in solution, the absorption or scattering properties of the molecule were monitored over time and at various temperatures.

UV kinetic properties were explored by solubilizing **BZ4** at 10 and 50 μM concentrations in a pseudo-physiological solution (PBS, pH 7.2) and acquiring the UV/Vis spectra of the obtained solutions at different times. Monitoring the UV spectrum of a 10 μM solution of **BZ4** in PBS over time showed that the absorption band at 314 nm was quite stable during the first 4 h after dissolution and the overall signal intensity decreased by 7.3% after 24 h (Supplementary Figure 5). These results could indicate the formation of some small aggregates that were not detectable by visual inspection. Aggregation of the compound was further confirmed by a more rapid and marked decrease of the absorption intensity over time when **BZ4** was solubilized in PBS at higher concentration (50 μM): the absorbance value at 314 nm decreased by 45% with respect to the original intensity after 5 h and by 76% after 24 h (SupplementaryFigure 6A). After stabilization of the UV absorption at 48 h, UV spectra were collected upon increasing the temperature to 85°C (Supplementary Figure6B). Interestingly, by maintaining the temperature at 85°C for 140 min, the UV signal recovered the initial intensity (Supplementary Figure 6C) and the UV spectrum at 85°C (Supplementary Figure 6D) was almost superimposable to the one at 25°C immediately after dissolution of the benzodifuran (t = 0; Supplementary Figure 6A), data indicative of the dissociation of the aggregates at high temperature.

This last datum, together with the consistency of the mass spectra of **BZ4** before and after the kinetic (0 to 48 h) and thermal (2.5 h at 85°C) experiments, allowed us to exclude decomposing processes of the compound, instead evidencing its good stability over time and temperature.

The formation of aggregates in a pseudo-physiological solution was further supported by the observed deviation from linearity of the 314 nm absorbance values of **BZ4** dissolved in PBS at different concentrations (Figure 5): the signal intensity increased linearly with the concentration up to about 20 μM, whereas at concentrations higher than 25 μM divergences from linearity were observed. With respect to the behavior of the previously reported benzodifuran derivatives [8], **BZ4** showed a higher solubility in aqueous media, as expected: indeed, the deviation from linearity of the UV absorbance versus concentration for **BZ1**, the more polar compound of the previous series, occurred already above 10 μM, and the stability of its UV signal with time denoted a faster reduction of the absorption band than in the case of **BZ4** [8]. Furthermore, from visual inspection of a set of freshly prepared solutions of the benzodifurans in PBS, we observed the presence of white suspensions for **BZ4** starting from 35 μM samples and for **BZ1** already at 20 μM: these data, in accordance with the UV results, provide evidence, with good approximation, that the aqueous solubility is ca. 3–4 × 10^{-5} M for **BZ4** and 1–2 × 10^{-5} M for **BZ1**, according to the values found for other polycyclic aromatic compounds [36].

In addition to UV spectroscopy, DLS provided insight into the ability of **BZ4** to self-aggregate, as evidenced for other benzodifurans [8]. Upon incubation at 25°C for 20 min at 10 μM concentration, DLS analysis showed aggregates with a size distribution composed of one prevailing population (93.3%) with average hydrodynamic

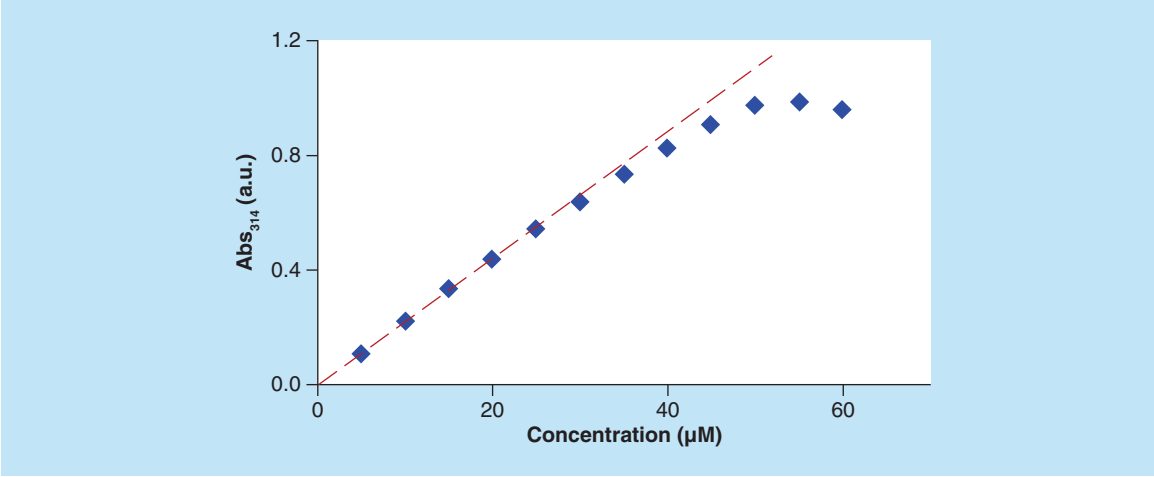

Figure 5. UV absorbance of BZ4 monitoring at 314 nm at different concentrations (5–60 μM) in phosphate-buffered saline (pH 7.2) at 25°C. The measurements were performed on freshly prepared solutions obtained by diluting **BZ4** in phosphate-buffered saline from concentrated stock solutions in DMSO (from 0.75 to a maximum of 9 mM), maintaining a constant DMSO concentration (0.67%), necessary to dissolve the samples.

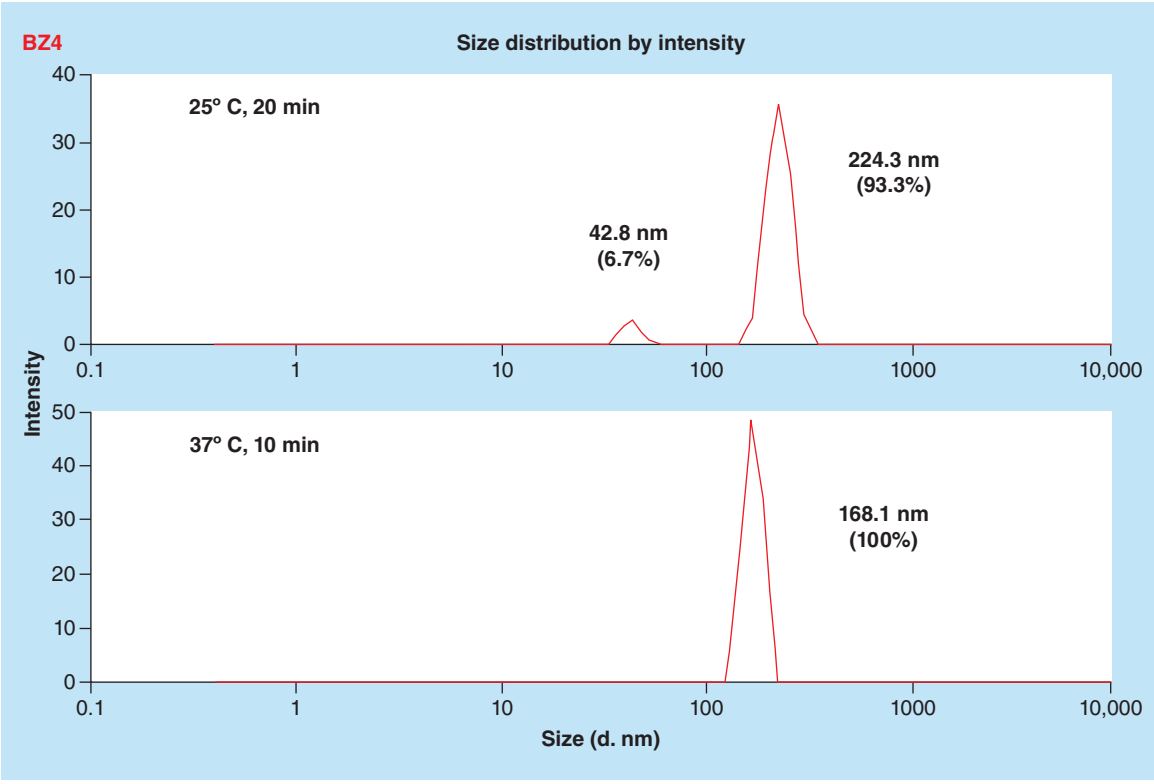

Figure 6. Representative dynamic light scattering spectra of BZ4 (at 10 μM concentration in phosphate-buffered saline solution) at different temperatures (25°C and 37°C). The time required for signal stabilization at each temperature investigated was also reported.

diameter of 224 nm and a small population (6.7%) of 42 nm (Figure 6). Upon incubation of these samples for 10 min at 37°C, a general reduction in the particle size was observed, with confluence of the system into a single narrow-shaped population having a size-distribution centered around 168 nm.

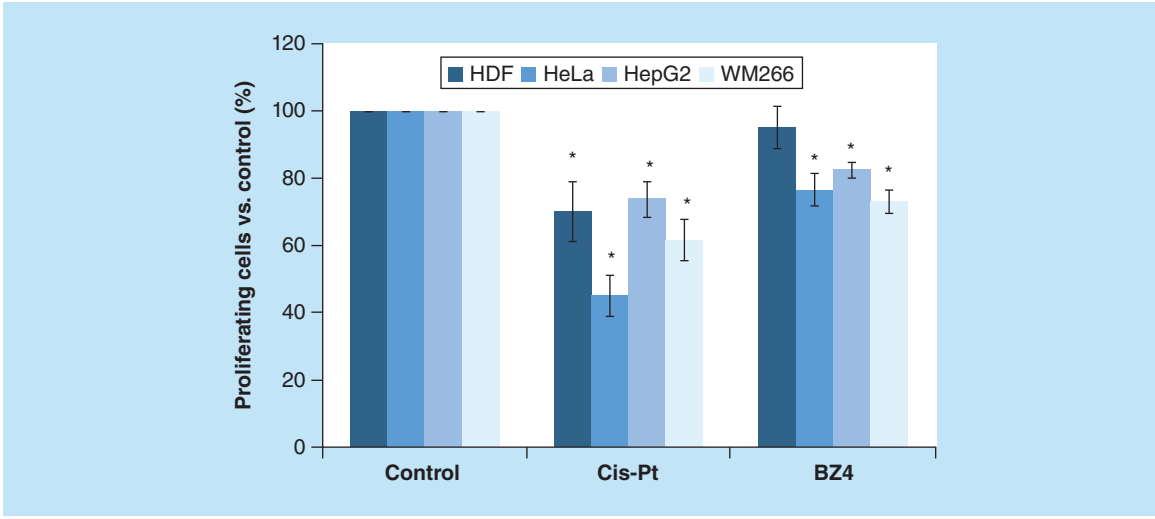

Figure 7. Cytotoxic effects of BZ4 on different cell lines in comparison with cisplatin. Cells were incubated with the tested compounds at 10 μM concentration at 37°C for 24 h. Proliferating cells are reported as percentage respect to the control (vehicle-treated cells) and are expressed as means ± SE. All the cell experiments on the antiproliferative activity of **BZ4** were carried out at least in triplicate. Statistical significance was analyzed using Student's t-test, unpaired and two-sided.
*$p < 0.05$.
HDF: Human dermal fibroblast; HeLa: Human cervix adenocarcinoma cells; HepG2: Liver hepatocellular cells; WM266: Malignant melanoma.

The aggregation ability found for **BZ4** could be due to its potential to form intermolecular interactions, as hypothesized on the basis of models (Supplementary Figure 1). Considering the molecular volume of **BZ4** estimated using the Molinspiration software (450.75 $Å^3$, Supplementary Table 1), leading to a molecular radius of 4.75 Å ($r = [3V/4\pi]^{1/3}$), and combining this result with the experimentally determined hydrodynamic radius of clusters formed by multiple **BZ4** units (at 10 μM concentration of the benzodifuran at 25°C), which is 112 nm (1120 Å) as deduced from DLS experiments, several hundreds of monomers form the supramolecular assembly of **BZ4**.

Antiproliferative activity of BZ4

The novel benzodifuran derivative **BZ4** was then tested for its antiproliferative activity using the MTT assay (Figure 7). Three human cancer cell lines (HeLa, Hep-G2 and WM266) and normal HDF were incubated with **BZ4** at 10 μM concentration for 24 h, using cisplatin at the same concentration as a positive control. While **BZ4** induced moderate cytotoxic activity on the three cancer cell lines, no effect was observed on HDF cells. In analogous experiments, cisplatin reduced the viability of normal HDF by 33%. This apparent selectivity, similar to what previously found for the other benzodifuran derivatives [8], makes **BZ4** an interesting starting compound to develop new potential anticancer drugs.

In order to elucidate the possible bioactivity mechanisms of **BZ4**, its ability to bind various DNA model systems and biologically relevant metal ions, as well its aggregation properties, were also evaluated.

Studies on the interaction with DNA

Oligonucleotide binders play a key role in the development of new anticancer drugs. For this reason, great interest has been recently devoted to the synthesis of molecules able to selectively bind with nucleic acids strands [37–40]. The interaction of **BZ4** with DNA in solution was here analyzed using the following model systems: three random coil single stranded ODNs (**A**, **B** and **C**); a bimolecular 12-mer duplex (from the association of complementary ODNs **A** and **B**) and a unimolecular G-quadruplex (G4) obtained by folding of a tract of the human telomere sequence (the 26-mer $\mathbf{tel_{26}}$), an important target in anticancer strategies. In particular, ODNs **A** and **B** contain consecutive purines in their sequence, while ODN **C** does not contain consecutive purines. All the interaction studies were carried out in a 100 mM KCl-phosphate buffer solution (pH 7.2), analogous to recent works [8,41,42].

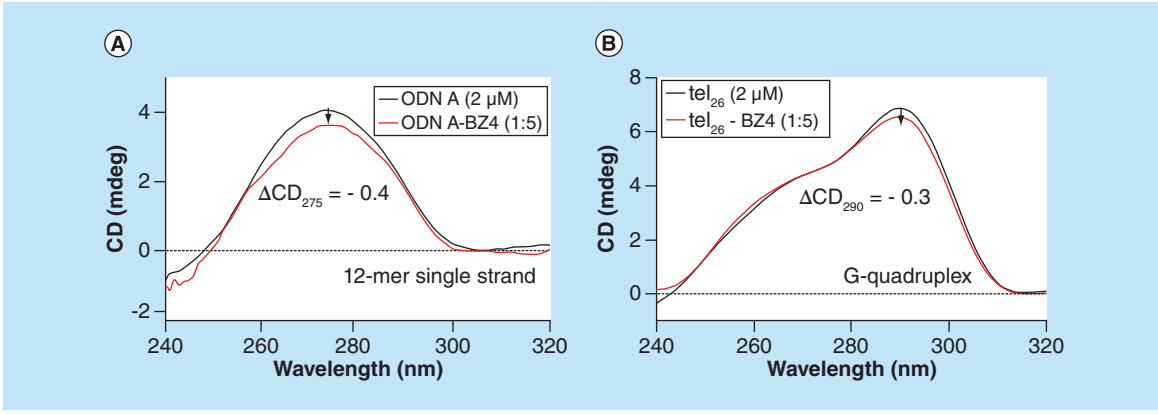

Figure 8. DNA binding spectroscopic studies. (A) Overlapping CD spectra of the single strand ODN and **(B)** the G4 tel_{26} (2 μM each) in the absence (black lines) and presence (red lines) of 5 equiv. of **BZ4**, in a 100 mM KCl-phosphate buffer solution (pH 7.2). Each titration was repeated three-times (the error on the calculated ΔCD value was ± 0.07 mdeg): in the figure a representative example for each system was reported.
CD: Circular dichroism; ODN: Oligodeoxyribonucleotide.

As the benzodifuran did not show a CD signal at the chosen concentrations (data not shown), CD titration experiments were carried out by adding increasing equivalents of **BZ4** to each selected DNA system (2 μM concentration). Thus, we monitored the difference in the CD spectrum of the ODNs after each addition. In Figure 8 and Supplementary Figure 7, the overlapped CD spectra of the ODN systems alone (black lines) and in the presence of five equivalents of **BZ4** (final point of the titration experiments, red curves) were reported.

Minor changes in the CD spectra of the single strands containing consecutive purines in the sequence (**A** and **B**; Figure 8A & Supplementary Figure 7A) were observed in the titrations, whereas no effect in the case of **C** (the ODN without consecutive purines; Supplementary Figure 7B) was found.

Regarding the structured systems, the titrations with **BZ4** produced little variations in the CD spectrum of the G-quadruplex structure (Figure 8B), whereas no effect on the duplex **A**/**B** was observed (Supplementary Figure 7C), demonstrating that in both cases no significant conformational change occurred.

However, CD melting experiments on the mixtures duplex-**BZ4** and **tel_{26}-BZ4** (obtained after the titration experiments) revealed a slight destabilization of the ODN secondary structures, reflected in T_m values 4 and 2°C lower than those of the untreated duplex and G-quadruplex, respectively (data not shown). These data demonstrated that **BZ4** is able to interact with the analyzed duplex and G-quadruplex systems, even if this occurs without significantly affecting their overall conformation and thermal stability. Thus it seems plausible to exclude a DNA-binding mechanism as the main mechanism of action for the observed antiproliferative activity of **BZ4**.

Ability of BZ4 to bind copper II ions

Considering the crucial role that copper plays in tumor progression [43] and the observed effect of copper chelators as anticancer drugs by blocking tumor angiogenesis and growth in animal models [44], we also investigated the capability of **BZ4** to bind copper(II) ions. The UV/Vis-monitored binding experiments were performed by incubating **BZ4** with two equivalents of a Cu^{2+} solution and then the spectra were recorded over a 3-h period.

As shown in Figure 9A, the incubation of **BZ4** with $CuCl_2$ for 20 min resulted in the appearance of a new band at 550 nm, indicative of copper (II) recognition in agreement with literature reports [45,46].

It is interesting to notice that also the homologous benzodifuran **BZ1** showed a similar behavior with copper II ions, whereas **BZ2** and **BZ3** were not able to bind Cu^{2+}, as we previously reported [8]. Analyzing the structures of all the benzodifurans (Figure 1) and their copper-binding ability, we concluded that the Cu^{2+} coordination involves the amino groups on furan rings, as well as the ether oxygen atoms of the ester chains.

Thus, in analogy to **BZ1** [8], we can hypothesize a hexacoordinated copper(II) dimeric complex (2 **BZ4** molecules per Cu^{2+}, Figure 9B), as repeating unit of a multimeric supramolecular network which could be arisen due to the symmetric nature of **BZ4**.

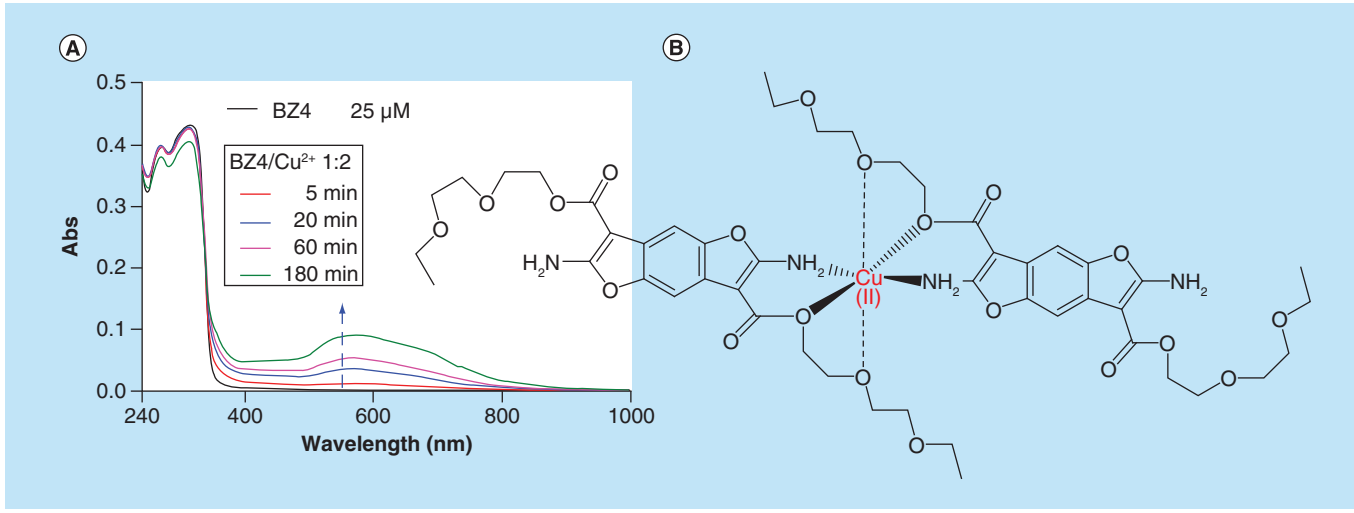

Figure 9. Copper (II) binding studies. (A) Overlapped UV spectra of a **BZ4** solution (25 μM) in PBS after signal stabilization (black line), and a solution containing both **BZ4** (25 μM) and $CuCl_2$ (50 μM) in phosphate-buffered saline at different time periods (5 min after Cu^{2+} addition = red line, 20 min = blue, 1 h = magenta, 3 h = green); **(B)** hypothesis of copper(II)-binding by **BZ4**.

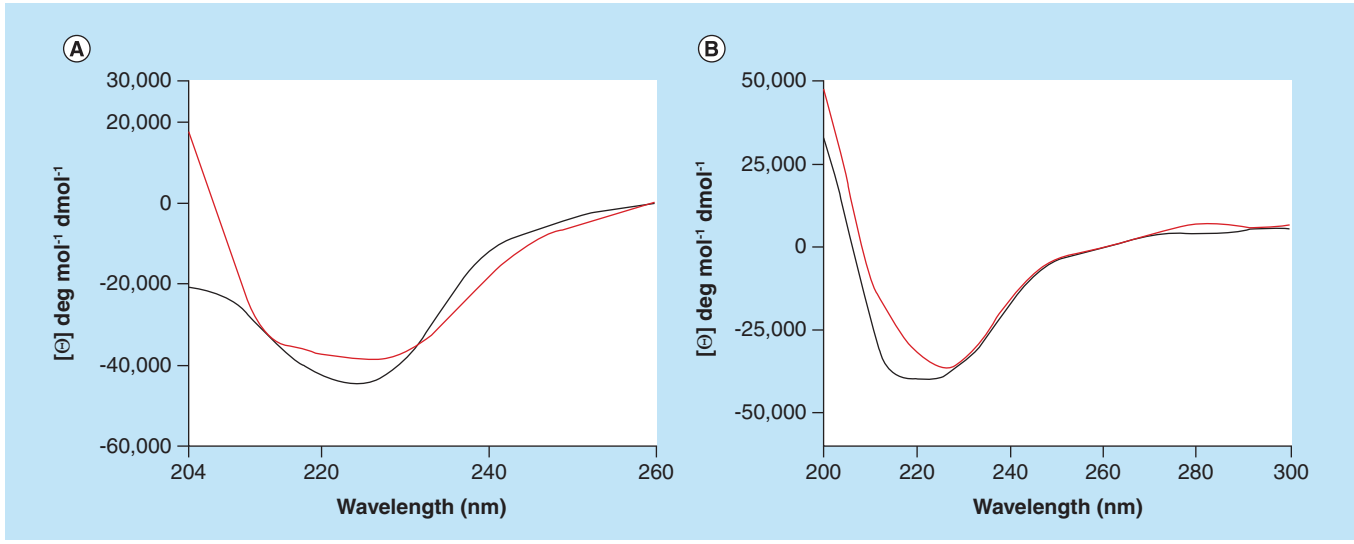

Figure 10. Circular dichroism studies on the interaction of amyloid peptide with BZ4. (A) Circular dichroism spectra of $A\beta_{42}$ (5 μM concentration in phosphate-buffered saline, black line) and $A\beta_{42}$ + **BZ4** (2 equiv., red line) after 24 h and **(B)** 48 h of incubation at 37°C.

Ability of BZ4 to interact with the amyloid peptide $A\beta_{42}$

Aβ peptide – the main constituent of plaques associated with AD – has been suggested to play an important role in AD. Here, we tested the ability of **BZ4** to interact with $A\beta_{42}$ peptide and interfere with its aggregation process. The aggregation of $A\beta_{42}$, incubated in PBS at 37°C, was monitored by CD spectroscopy at different times (0, 24 and 48 h). The spectra obtained at the different incubation times showed changes similar to those reported in literature [47].

In parallel, $A\beta_{42}$ was incubated at 37°C in the presence of **BZ4** (which did not show any contribution to the CD signal) and CD spectra at different incubation times were recorded. When comparing the obtained CD spectra after 24 and 48 h of incubation it became apparent that the presence of **BZ4** induced differences in the structural organization of $A\beta_{42}$. (Figure 10). The spectral changes, impacting both intensity and shape of the negative valley at 225 nm already described by Guo *et al.* [48], suggested that **BZ4** partly suppresses the β-sheet structure of $A\beta_{42}$ leading to new structural elements.

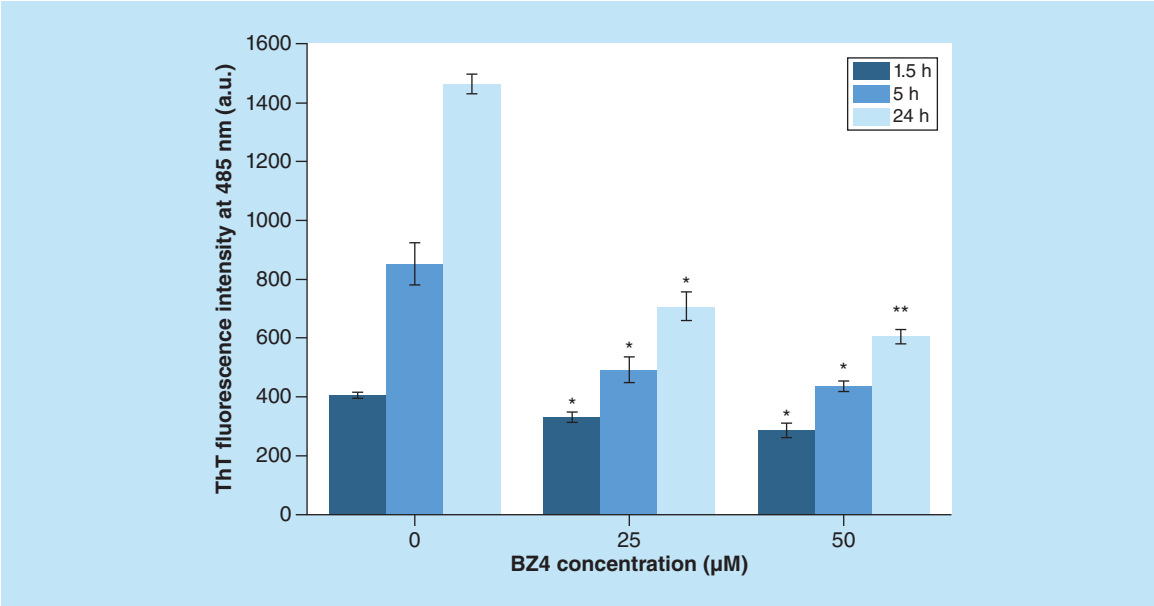

Figure 11. BZ4 exerts a dose-dependent inhibiting effect on the amyloid fibril formation of $A\beta_{42}$. Solutions containing $A\beta_{42}$ at a concentration of 25 μM were incubated in the presence and absence of **BZ4** at 37°C for 1.5, 5 and 24 h. Amyloid fibril formation was detected using ThT fluorescence intensity measurements at a detection wavelength of 485 nm. The reported values represent the results obtained from three independent experiments. The statistical significance of the replicates was assessed by p-values using paired two-tailed t-tests (GraphPad Software). *$p < 0.05$; **$p < 0.005$.

Ability of BZ4 to interfere with Aβ aggregation propensity

The potential interaction between **BZ4** and $A\beta_{42}$ suggests the possibility that **BZ4** may also impact on the aggregation of this peptide. Aggregation of $A\beta_{42}$ was monitored at different times (1.5, 5 and 24 h) upon incubation at 37°C in the presence or absence of **BZ4** using ThT fluorescence. ThT is a dye commonly used to measure the aggregation propensity of $A\beta_{42}$, as it generates a characteristic fluorescence emission upon binding to amyloid β-sheet structures [47,49]. The incubation of the peptide alone generated an increase in the fluorescence over time, indicating that the peptide self-assembled into ThT-binding fibrils. On the other hand, when $A\beta_{42}$ was incubated with **BZ4** at various concentrations, fibril formation was significantly inhibited in a dose-dependent manner, as shown by the lower ThT fluorescence intensities (Figure 11). In particular, **BZ4** was active at concentrations exceeding 25 μM and after 5 h incubation.

Anti-aggregation activity of **BZ4** was compared with those of the previously synthesized benzodifuran derivatives of Figure 1 [8]. Interestingly, compounds **BZ1**, **BZ2** and **BZ3** showed no significant inhibitory activity, demonstrating that the specific structural features of **BZ4** are essential for this effect (Supplementary Figures 8–10).

Having found this activity only for **BZ4**, in view of further exploring its potential as a therapeutic agent in neurodegenerative diseases, we tested its cytotoxicity on primary mouse cortical neurons using the MTT assay. We found that **BZ4** was nontoxic up to a concentration of 20 μM, compared with cytotoxic staurosporine (Figure 12).

Interestingly, in analogy to **BZ4**, another polycyclic aromatic compound, imidazoquinoline dactolisib (NVP-BEZ235), showed antiproliferative activity [50], as well as significant neuroprotective effects as evidenced in studies carried out on the Aβ [51]. The dual activity of dactolisib relies on the PI3K/mTOR pathway involved in protection against neurodegeneration in hippocampal neuronal cultures and mice while inducing an antiproliferative effect [51].

SEM analysis of aggregated Aβ morphology in absence & presence of BZ4

The effect of **BZ4** on the morphology of $A\beta_{42}$ aggregates was investigated after 48 h incubation at 37°C by SEM.

The SEM micrograph depicted in Figure 13A showed the surface morphology of pure **BZ4** crystals: only a regular roughness of about 10 nm appeared. $A\beta_{42}$ incubated for 48 h at 37°C (in PBS solution at pH 7.2) in the absence of compound **BZ4** showed both a granular morphology (Figure 13B), and filaments of considerable length (Figure 13C) and with thickness in the range 20–30 nm (Figure 13D), visible on the surface, in line with previous

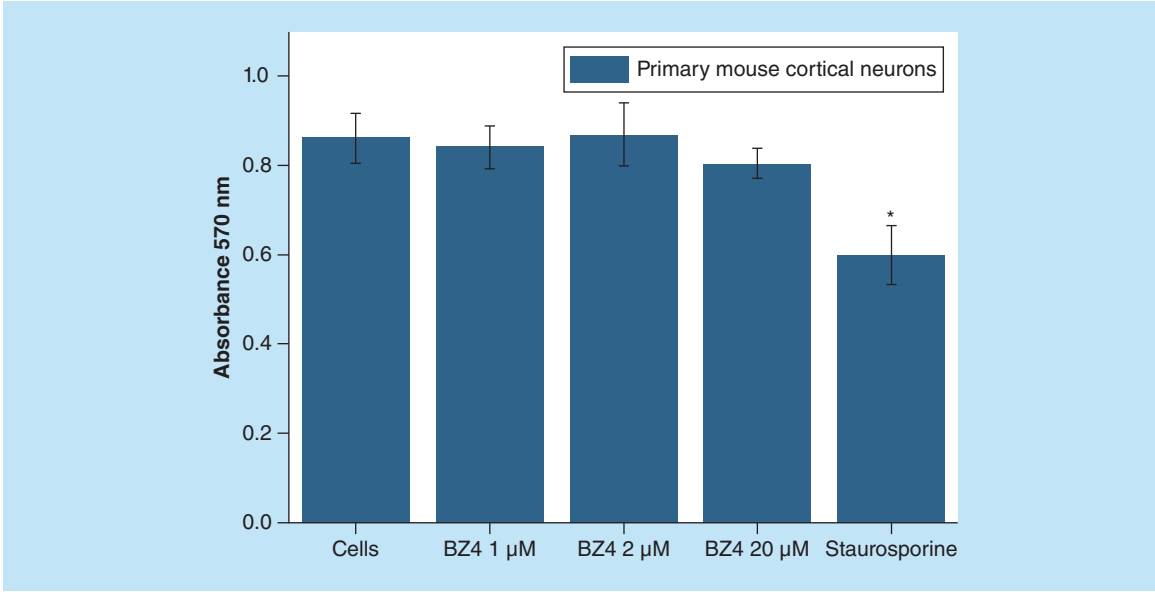

Figure 12. Cell viability assay using the MTT protocol on primary mouse cortical neurons exposed to 1, 2 and 20 µM concentrations of BZ4. A 2 µM solution of staurosporine and nontreated cells were used, respectively, as negative and positive controls. Statistical significance was analyzed using student's t-test, unpaired and two-sided. All the experiments were performed in triplicate
*$p < 0.01$

reports [52]. After incubation of $A\beta_{42}$ with **BZ4** under the same experimental conditions, SEM micrographs of the mixture evidenced a different granular morphology with visual absence of filamentous materials (Figure 13E). Thus, SEM analysis demonstrated an altered morphology of $A\beta_{42}$ in samples where **BZ4** was present with respect to those only containing the pure Aβ peptide, with disappearance of the typical filaments.

Conclusion

In this paper, we report the synthesis and characterization of a new benzodifuran derivative, named **BZ4**, and the evaluation of its biological properties, including anticancer and anti-amyloid activities, as well as its ability to interact with several DNA model systems. **BZ4** was designed starting from a previously reported benzodifuran derivative (**BZ1**), showing promising biological activities, by elongating the two oligoethylene glycol chains, with the aim of improving its solubility in aqueous solutions and, in general, the hydrophilic–lipophilic balance of the molecule. The newly synthesized compound showed significant antiproliferative activity on a panel of human cancer cells, but not on normal HDF or primary neuronal cells. Analogously to the previously tested benzodifuran derivatives [8], the antiproliferative activity of **BZ4** could be connected to the formation of nanoaggregates, evidenced by UV-vis spectroscopy and DLS analysis, as reported in other literature examples for several anticancer drugs [53]. Another interesting property of this compound is its ability to act as a copper (II) ion chelator, as the rameic cation binding was clearly evidenced by UV. In addition, thioflavin T fluorescence assays showed that **BZ4** inhibits, in a dose-dependent manner, aggregation of the Aβ peptide, one of the most relevant targets in current therapeutic strategies to treat AD. Instead, fibril formation was not significantly affected by **BZ1** and **BZ2**, and was potentiated by incubation of Aβ peptide with the most apolar derivative of the benzodifuran series (**BZ3**). The interaction of **BZ4** with Aβ was also confirmed by CD spectroscopy and SEM microscopy. These aspects, along with the absence of toxicity on neuronal primary cells, provide an interesting picture of the properties of this compound. This novel species could be a valuable core scaffold to generate libraries of optimized analogs in the search for new anticancer and anti-Alzheimer drugs investigating the final benzodifuran effective extra- and/or intracellular targets and its potential mechanism of action.

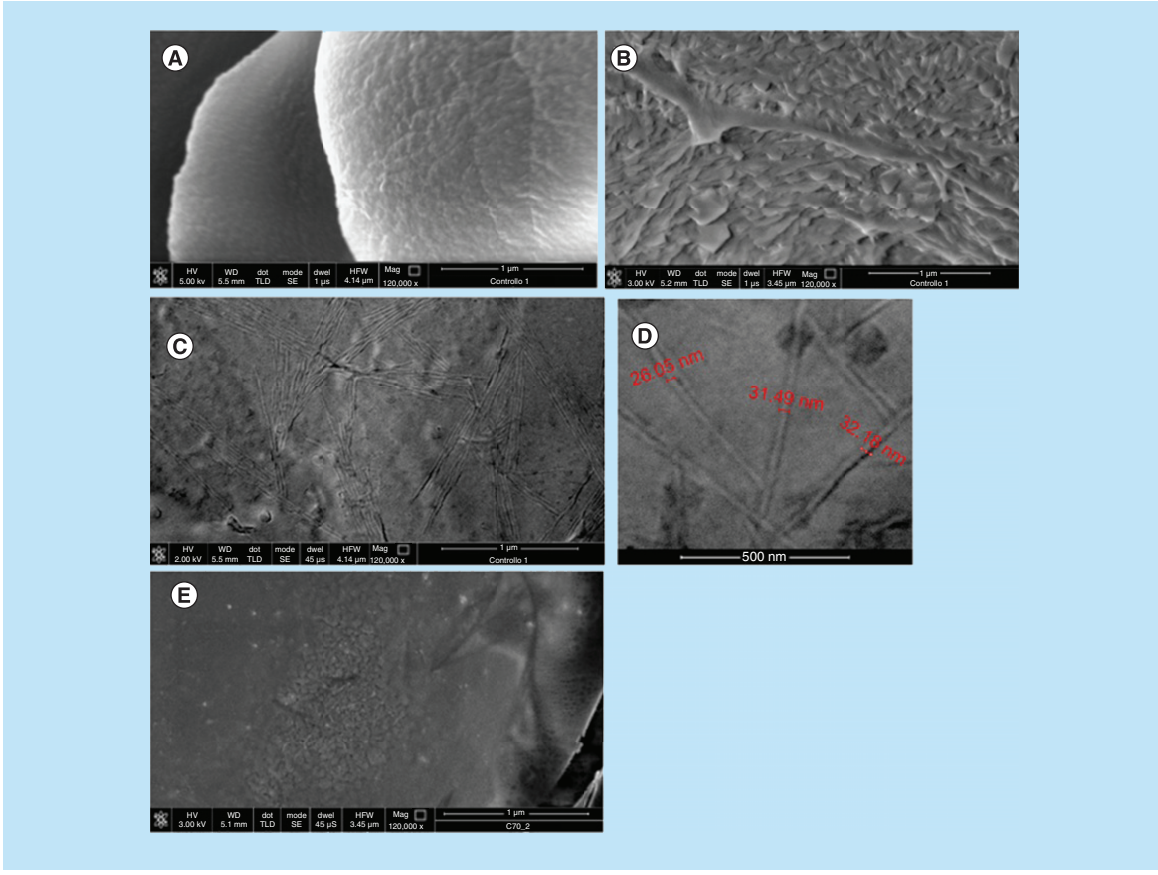

Figure 13. Scanning electron micrographs of Aβ with and without BZ4. (A) Pure **BZ4** (crystals); **(B)** granules and **(C)** filaments of $A\beta_{42}$; **(D)** detail of C ($A\beta_{42}$) and **(E)** $A\beta_{42}$ in presence of **BZ4**.
HFW: Horizontal field width; HV: High voltage; Mag: Magnification; Se: Secondary electron; TLD: Through the lens detector; WD: Working distance.

Future perspective

Overall, these findings indicate **BZ4** as a valuable scaffold to evolve potential candidate drugs for anticancer and Aβ-associated neuropathies and strongly encourage further efforts in the search for benzodifuran derivatives with pharmacological activity.

Besides the therapeutic applications that could derive from the present work, in future also the diagnostic potential of benzodifurans in disease imaging could be investigated, in analogy to previous reports on aromatic molecule applications in this area [54–58].

Supplementary data

See online at: www.future-science.com/doi/full/10.4155/fmc-2018-0473

Acknowledgments

We are grateful to A Roviello, Federico II University, Naples for his precious suggestions on the synthesis and characterization of **BZ4**. We also thank U Eisel and D Dekens, University of Groningen, for technical assistance in performing the primary neuronal cell culture assays.

Financial & competing interests disclosure

Thanks to ZonMw Memorabel for the financial support in buying the peptide and chemicals for the experiments performed in The Netherlands. This work was supported by the Italian Association for Cancer Research (AIRC) (IG2015 n. 17037 to D.M.) and Ministero dell'Istruzione, dell'Università e della Ricerca (MIUR) [grant number PON03PE_00060_4]. The authors have no other

relevant affiliations or financial involvement with any organization or entity with a financial interest in or financial conflict with the subject matter or materials discussed in the manuscript apart from those disclosed.

No writing assistance was utilized in the production of this manuscript.

Ethical conduct

The authors state that they have obtained appropriate institutional review board approval or have followed the principles outlined in the Declaration of Helsinki for all human or animal experimental investigations.

Summary points

- In the context of the biological evaluation of benzodifuran compounds, this study reports on the synthesis, characterization and bioactivity of a new derivative, named **BZ4**.
- This compound showed antiproliferative activity on a panel of human cancer cells, but no significant cytotoxicity on normal human dermal fibroblast or primary neuronal cells.
- The antiproliferative activity of **BZ4** could be connected to the formation of nanoaggregates, evidenced by UV-Vis spectroscopy and dynamic light scattering analysis, and/or with its ability to act as a copper (II) ion chelator, demonstrated by UV studies.
- Thioflavin T fluorescence assays, as well as circular dichroism and scanning electron microscopy analyses, showed that **BZ4** interacts with the β-amyloid (Aβ) peptide altering its structure and morphology, and interfering with its aggregation properties.

References

Papers of special note have been highlighted as: • of interest; •• of considerable interest

1. Li XY, He BF, Luo HJ, Huang NY, Deng WQ. 3-acyl-5-hydroxybenzofuran derivatives as potential anti-estrogen breast cancer agents: a combined experimental and theoretical investigation. *Bioorganic Med. Chem. Lett.* 23(16), 4617–4621 (2013).

• **Highlights the potential of benzofuran derivatives as anticancer drugs.**

2. Briest S, Davidson NE. Aromatase inhibitors for breast cancer. *Rev. Endocr. Metab. Disord.* 8(3), 215–228 (2007).
3. Khodarahmi GA, Smith HJ, Nicholls PJ, Ahmadi M. Enantioselectivity of some 1-(benzofuran-2-yl)-1-(1-H-imidazol-1-yl) alkanes as inhibitors of P450. *J. Pharm. Pharmacol.* 50(11), 1321–1330 (1998).
4. Du Z, Chen Y, Chen W *et al.* Development of new two-dimensional small molecules based on benzodifuran for efficient organic solar cells. *Chem. Asian J.* 9(9), 2621–2627 (2014).
5. Soni JN, Soman SS. Synthesis and antimicrobial evaluation of amide derivatives of benzodifuran-2-carboxylic acid. *Eur. J. Med. Chem.* 75, 77–81 (2014).
6. Feng Z, Mohapatra S, Klimko PG *et al.* Novel benzodifuran analogs as potent 5-HT2A receptor agonists with ocular hypotensive activity. *Bioorganic Med. Chem. Lett.* 17(11), 2998–3002 (2007).
7. Viano I, Dianzani C, Gia O, Gastaldi S, Genazzani E. Biological properties of benzodifuran derivatives. *Drugs Exp. Clin. Res.* 11(12), 865–867 (1985).

• **Highlights the nucleic-acid associated biological properties of benzodifuran derivatives.**

8. Musumeci D, Roviello GN, Rigione G *et al.* Benzodifuran derivatives as potential antiproliferative agents: possible correlation between their bioactivity and aggregation properties. *Chempluschem* 82(2), 251–260 (2017).

•• **This is a key work on the relationships beween bioactivity and chemistry of benzodifuran compounds.**

9 . Molina-Guijarro JM, Macías Á, García C *et al.* Irvalec inserts into the plasma membrane causing rapid loss of integrity and necrotic cell death in tumor cells. *PLoS ONE* 6(4), doi:https://doi.org/10.1371/journal.pone.0019042 (2011) (Epub ahead of print).

10. Musumeci D, Irace C, Santamaria R, Milano D, Tecilla P, Montesarchio D. Guanine-based amphiphiles: synthesis, ion transport properties and biological activity. *Bioorganic Med. Chem.* 23(5), 1149–1156 (2015).
11. Simeone L, Mangiapia G, Irace C *et al.* Nucleolipid nanovectors as molecular carriers for potential applications in drug delivery. *Mol. Biosyst.* 7(11), 3075–3086 (2011).
12. Licen S, Coppola C, D'Onofrio J, Montesarchio D, Tecilla P. CyPLOS: a new family of synthetic ionophores. *Org. Biomol. Chem.* 7(6), 1060–1063 (2009).
13. Roviello GN, Iannitti R, Palumbo R, Simonyan H, Vicidomini C, Roviello V. Lac-L-TTA, a novel lactose-based amino acid–sugar conjugate for anti-metastatic applications. *Amino Acids* 49(8), 1347–1353 (2017).
14. Roviello GN, Iannitti R, Roviello V, Palumbo R, Simonyan H, Vicidomini C. Synthesis and biological evaluation of a novel Amadori compound. *Amino Acids.* 49(2), 327–335 (2017).

15. Kuperstein I, Broersen K, Benilova I *et al.* Neurotoxicity of Alzheimer's disease Aβ peptides is induced by small changes in the Aβ42 to Aβ40 ratio. *EMBO J.* 29(19), 3408–3420 (2010).
16. Rajasekhar K, Chakrabarti M, Govindaraju T. Function and toxicity of amyloid beta and recent therapeutic interventions targeting amyloid beta in Alzheimer's disease. *Chem. Commun.* 51(70), 13434–13450 (2015).
17. Doig AJ, Derreumaux P. Inhibition of protein aggregation and amyloid formation by small molecules. *Curr. Opin. Struct. Biol.* 30, 50–56 (2015).
18. Knowles TPJ, Vendruscolo M, Dobson CM. The amyloid state and its association with protein misfolding diseases. *Nat. Rev. Mol. Cell Biol.* 15(6), 384–396 (2014).
19. Scherzer-Attali R, Pellarin R, Convertino M *et al.* Complete phenotypic recovery of an Alzheimer's disease model by a quinone–tryptophan hybrid aggregation inhibitor. *PLoS ONE* 5(6) doi:https://doi.org/10.1371/journal.pone.0011101 (2010) (Epub ahead of print).
20. Yang F, Lim GP, Begum AN *et al.* Curcumin inhibits formation of amyloid β oligomers and fibrils, binds plaques, and reduces amyloid *in vivo*. *J. Biol. Chem.* 280(7), 5892–5901 (2005).
21. Shu B, Zhang X, Du G, Fu Q, Huang L. MicroRNA-107 prevents amyloid-β-induced neurotoxicity and memory impairment in mice. *Int. J. Mol. Med.* 41(3), 1665–1672 (2018).
22. Salvati E, Re F, Sesana S *et al.* Liposomes functionalized to overcome the blood–brain barrier and to target amyloid-β peptide: the chemical design affects the permeability across an *in vitro* model. *Int. J. Nanomed.* 8, 1749–1758 (2013).
23. Kisilevsky R, Lemieux LJ, Fraser PE, X K, Hultin PG, Szarek WA. Arresting amyloidosis *in vivo* using small-molecule anionic sulphonates or sulphates: implications for Alzheimer's disease. *Nat. Med.* 1(2), 143–148 (1995).
24. Han SH, Chang YJ, Jung ES, Kim JW, Na DL, Mook-Jung I. Effective screen for amyloid β aggregation inhibitor using amyloid β-conjugated gold nanoparticles. *Int. J. Nanomed.* 6(1), 1–12 (2011).
25. Ono M, Kawashima H, Nonaka A *et al.* Novel benzofuran derivatives for PET imaging of beta-amyloid plaques in Alzheimer's disease brains. *J. Med. Chem.* 49(9), 2725–2730 (2006).
26. González-Ramírez M, Gavilán J, Silva-Grecchi T *et al.* A natural benzofuran from the patagonic aleurodiscus vitellinus fungus has potent neuroprotective properties on a cellular model of amyloid-β peptide toxicity. *J. Alzheimer's Dis.* 61(4), 1463–1475 (2018).
27. Choi H, Seo P, Son B, Kang B. Synthesis of 5-Chloro-3-[4-(3-diethylaminopropoxy)benzoyl]-2- (4-methoxyphenyl)benzofuran as a β-amyloid aggregation inhibitor. *Arch. Pharm. Res.* 26(12), 985–989 (2003).
28. Rosini M, Simoni E, Bartolini M *et al.* Inhibition of acetylcholinesterase, β-amyloid aggregation, and NMDA receptors in Alzheimer's disease: a promising direction for the multi-target-directed ligands gold rush. *J. Med. Chem.* 51(15), 4381–4384 (2008).
29. Howlett DR, Perry AE, Godfrey F *et al.* Inhibition of fibril formation in beta-amyloid peptide by a novel series of benzofurans. *Biochem. J.* 340(Pt. 1), 283–289 (1999).
30. Ono M, Kung MP, Hou C, Kung HF. Benzofuran derivatives as Aβ-aggregate-specific imaging agents for Alzheimer's disease. *Nucl. Med. Biol.* 29(6), 633–642 (2002).
31. Platella C, Guida S, Bonmassar L *et al.* Antitumour activity of resveratrol on human melanoma cells: a possible mechanism related to its interaction with malignant cell telomerase. *Biochim. Biophys. Acta Gen. Subj.* 1861(11), 2843–2851 (2017).
32. Di Natale C, Scognamiglio PL, Cascella R *et al.* Nucleophosmin contains amyloidogenic regions that are able to form toxic aggregates under physiological conditions. *FASEB J.* 29(9), 3689–3701 (2015).
33. Roviello GN, Di Gaetano S, Capasso D, Cesarani A, Bucci EM, Pedone C. Synthesis, spectroscopic studies and biological activity of a novel nucleopeptide with Moloney murine leukemia virus reverse transcriptase inhibitory activity. *Amino Acids* 38(5), 1489–1496 (2010).
34. Pane K, Sgambati V, Zanfardino A *et al.* A new cryptic cationic antimicrobial peptide from human apolipoprotein E with antibacterial activity and immunomodulatory effects on human cells. *FEBS J.* 283(11), 2115–2131 (2016).
35. Broersen K, Jonckheere W, Rozenski J *et al.* A standardized and biocompatible preparation of aggregate-free amyloid beta peptide for biophysical and biological studies of Alzheimers disease. *Protein Eng. Des. Sel.* 24(9), 743–750 (2011).
36. Bohon RL, Claussen WF. The solubility of aromatic hydrocarbons in water. *J. Am. Chem. Soc.* 73(4), 1571–1578 (1951).
37. Roviello GN, Musumeci D. Synthetic approaches to nucleopeptides containing all four nucleobases, and nucleic acid-binding studies on a mixed-sequence nucleo-oligolysine. *RSC Adv.* 6(68), 63578–63585 (2016).
38. Roviello GN, Vicidomini C, Di Gaetano S, Capasso D, Musumeci D, Roviello V. Solid phase synthesis and RNA-binding activity of an arginine-containing nucleopeptide. *RSC Adv.* 6(17), 14140–14148 (2016).
39. Roviello GN, Vicidomini C, Costanzo V, Roviello V. Nucleic acid binding and other biomedical properties of artificial oligolysines. *Int. J. Nanomed.* 11, 5897–5904 (2016).
40. Roviello GN, Musumeci D, Bucci EM, Pedone C. Synthesis and characterization of a novel ester-based nucleoamino acid for the assembly of aromatic nucleopeptides for biomedical applications. *Int. J. Pharm.* 415(1–2), 206–210 (2011).
41. Musumeci D, Platella C, Riccardi C *et al.* A first-in-class and a fished out anticancer platinum compound: cis-$[PtCl_2(NH_3)_2]$ and cis-$[PtI_2(NH_3)_2]$ compared for their reactivity towards DNA model systems. *Dalt. Trans.* 45(2), 8587–8600 (2016).

42. Musumeci D, Rozza L, Merlino A *et al.* Interaction of anticancer Ru(III) complexes with single stranded and duplex DNA model systems. *Dalton Trans.* 44(31), 13914–25 (2015).
43. Denoyer D, Masaldan S, La Fontaine S, Cater MA. Targeting copper in cancer therapy: "Copper That Cancer." *Metallomics* 7(11), 1459–1476 (2015).
44. Pan Q, Kleer CG, Van Golen KL *et al.* Copper deficiency induced by tetrathiomolybdate suppresses tumor growth and angiogenesis. *Cancer Res.* 62(17), 4854–4859 (2002).
45. Wu J, Wang Y, Wang Y *et al.* Cu^{2+}-RG DFRG DS: exploring the mechanism and high efficacy of the nanoparticle in antithrombotic therapy. *Int. J. Nanomed.* 10, 2925–2938 (2015).
46. Kaur K, Kumar S. Dansyl-anthracene dyads for ratiometric fluorescence recognition of Cu^{2+}. *Dalt. Trans.* 40(11), 2451–2458 (2011).
47. Dai X, Hou W, Sun Y, Gao Z, Zhu S, Jiang Z. Chitosan oligosaccharides inhibit/disaggregate fibrils and attenuate amyloid β-mediated neurotoxicity. *Int. J. Mol. Sci.* 16(5), 10526–10536 (2015).
48. Guo J, Sun W, Li L, Liu F, Lu W. Brazilin inhibits fibrillogenesis of human islet amyloid polypeptide, disassembles mature fibrils, and alleviates cytotoxicity. *RSC Adv.* 7(69), 43491–43501 (2017).
49. Biancalana M, Koide S. Molecular mechanism of thioflavin-T binding to amyloid fibrils matthew. *Biochim Biophys Acta* 1804(7), 1405–1412 (2010).
50. Serra V, Markman B, Scaltriti M *et al.* NVP-BEZ235, a dual PI3K/mTOR inhibitor, prevents PI3K signaling and inhibits the growth of cancer cells with activating PI3K mutations. *Cancer Res.* 68(19), 8022–8030 (2008).
51. Bellozi PMQ, Lima IV de A, Dória JG *et al.* Neuroprotective effects of the anticancer drug NVP-BEZ235 (dactolisib) on amyloid-β1-42 induced neurotoxicity and memory impairment. *Sci. Rep.* 6, 25226 (2016).
52. Picone P, Carrotta R, Montana G, Nobile MR, San Biagio PL, Di Carlo M. Aβ oligomers and fibrillar aggregates induce different apoptotic pathways in LAN5 neuroblastoma cell cultures. *Biophys. J.* 96(10), 4200–4211 (2009).
53. Tanaka A, Fukuoka Y, Morimoto Y *et al.* Cancer cell death induced by the intracellular self-assembly of an enzyme-responsive supramolecular gelator. *J. Am. Chem. Soc.* 137(2), 770–775 (2015).
54. Wang W, Mao Z, Wang M *et al.* A long lifetime luminescent iridium(III) complex chemosensor for the selective switch-on detection of Al^{3+} ions. *Chem. Commun.* 52(18), 3611–3614 (2016).
55. Vicidomini C, Panico M, Greco A *et al. In vivo* imaging and characterization of [18F]DPA-714, a potential new TSPO ligand, in mouse brain and peripheral tissues using small-animal PET. *Nucl. Med. Biol.* 42(3), 309–316 (2015).
56. Ma DL, Lin S, Leung KH *et al.* An oligonucleotide-based label-free luminescent switch-on probe for RNA detection utilizing a G-quadruplex-selective iridium(III) complex. *Nanoscale* 6(15), 8489–8494 (2014).
57. Leung KH, He HZ, Chan DSH, Fu WC, Leung CH, Ma DL. An oligonucleotide-based switch-on luminescent probe for the detection of kanamycin in aqueous solution. *Sens. Actuators B Chem.* 177, 487–492 (2013).
58. Carella A, Roviello V, Iannitti R *et al.* Evaluating the biological properties of synthetic 4-nitrophenyl functionalized benzofuran derivatives with telomeric DNA binding and antiproliferative activities. *Int. J. Biol. Macromol.* 121, 77–88 (2018).